JGR Oceans

RESEARCH ARTICLE
10.1029/2020JC017018

Insight Into the Dynamics of the Radiating Internal Tide Associated With the Kuroshio Current

Zhenhua Xu[1,2,3,4], Yang Wang[1,2,3,4], Zhiqiang Liu[5], James C. McWilliams[6], and Jianping Gan[7]

[1]CAS Key Laboratory of Ocean Circulation and Waves, Institute of Oceanology Chinese Academy of Sciences, Qingdao, China, [2]Pilot National Laboratory for Marine Science and Technology, Qingdao, China, [3]Center for Ocean Mega-Science, Chinese Academy of Sciences, Qingdao, China, [4]College of Earth and Planetary Sciences, University of Chinese Academy of Sciences, Beijing, China, [5]Department of Ocean Science and Engineering, Southern University of Science and Technology, Shenzhen, China, [6]Department of Atmospheric and Oceanic Sciences, University of California, Los Angeles, CA, USA, [7]Department of Mathematics and Department of Ocean Science, The Hong Kong University of Science and Technology, Hong Kong, China

Key Points:

- Interaction between the internal tide in Luzon Strait and Kuroshio greatly affects internal tidal energy field
- We obtain an unprecedented observation-supported internal tidal energy field around Luzon Strait
- Radiating tidal pattern, dissipation efficiency, and energy field respond differently to the leaping, looping, and leaking Kuroshio paths

Correspondence to:
J. Gan,
magan@ust.hk

Citation:
Xu, Z., Wang, Y., Liu, Z., McWilliams, J. C., & Gan, J. (2021). Insight into the dynamics of the radiating internal tide associated with the Kuroshio Current. *Journal of Geophysical Research: Oceans*, *126*, e2020JC017018. https://doi.org/10.1029/2020JC017018

Received 27 NOV 2020
Accepted 3 MAY 2021

Abstract Ocean circulation strongly influences how internal tides radiate and break and stimulates the spatial inhomogeneity and temporal variation of internal tidal mixing. Qualitative and quantitative characterizations of interactions between internal tides and general circulation are critical to multi-scale circulation dynamics. Based on significant progress in regional circulation simulation, we obtain an observation-supported internal tide energy field around Luzon Strait by deterministically resolving the dynamics of the radiating paths of the internal tide energy. These paths are created when the known most powerful internal tide of Luzon Strait interacts with the Kuroshio Current. We found that the radiating tidal pattern, local dissipation efficiency, and energy field respond differently to the leaping, looping, and leaking Kuroshio paths within Luzon Strait. Our new insights into the dynamics and our clarifying the controlling refraction mechanism within the general circulation create the potential for internal tides to be represented better in climate models.

Plain Language Summary Internal tides drive oceanic mixing that varies spatially and temporally. This mixing crucially impacts how different ocean layers are maintained and drives overturning circulation of the global ocean's conveyor belt. Furthermore, the ocean's general circulation itself strongly influences how the internal tides radiate and break, which, in turn, stimulate variable turbulent mixing. Luzon Strait, which is between Taiwan and the Philippines, features the most powerful internal tides in the world. The strait also lies in the path of the strong western boundary Kuroshio Current as the current flows northeastward. In the last decade, Luzon Strait has been the global benchmarking site for internal wave studies. By numerically simulating the various paths and the variability of the Kuroshio Current that flows within Luzon Strait, we obtained an internal tide energy field that we validated with observations. Lastly, we proposed an evaluation criterion to theoretically clarify the refraction mechanism that controls how the internal tide radiates within general oceanic circulation. These new insights help us understand and represent internal tide energetics, tidal mixing, and the circulation energy spectrum in climate-scale models.

1. Introduction

Internal tides, generated by barotropic tidal currents flowing over abrupt topographic features (such as sills), are internal gravity waves that oscillate at tidal frequencies. The dissipating energy carried by propagating internal tides contribute a significant amount of mechanical energy to abyssal mixing and, hence, the general circulation (Polzin et al., 1997). For example, internal tides with spatial inhomogeneity and temporal variability largely induce a globally averaged diapycnal diffusivity of 10^{-4} m^2/s (Koch-Larrouy et al., 2010), which maintains global meridional overturning circulation (Garrett & Kunze, 2007). Therefore, to fully understand tidal mixing, it is crucial to dynamically resolve how fast-manifold internal tides radiate and how the tidal energy influence a balanced general circulation (Sprintall et al., 2014; Vlasenko et al., 2005; Whalen et al., 2018).

Most research efforts have been devoted to investigating internal tides without considering the background circulation or the background circulation was misrepresented in the studies. In the real ocean, the dynamics of internal tides are not solitary; the dynamics interact closely with the balanced circulation and other unbalanced flows (Chang et al., 2019; Dunphy & Lamb, 2014; McWilliams, 2016; Susanto et al., 2007; Varlamov et al., 2015). It is still challenging to qualitatively interpret and quantitatively resolve the energy budget and radiating patterns of the internal tides because of complex multi-scale interactions of circulation and the underlying physics (Jan et al., 2012; Qiu et al., 2017; Zhao et al., 2016). The complex interaction between the internal tides and the circulation hinders a deeper understanding of multi-scale oceanic processes; and a coordinated observation-modeling-theory effort to break the processes down does not exist (Kelly et al., 2016; Xu et al., 2013; Zaron & Egbert, 2014).

Luzon Strait (LS) has long been recognized as the most powerful source of internal tides in the World Ocean. The internal waves generated in LS are uniquely large and interact with the western boundary Kuroshio Current that flows northward and partially intrudes into the South China Sea (SCS) via LS (Alford et al., 2011, 2015; Buijsman, Kanarska, et al., 2010; Buijsman, McWilliams, et al., 2010; Pickering et al., 2015). The Internal Waves in Straits Experiment identified the important effects of the double-ridge topography and of the temporally variable Kuroshio on the internal tidal energetics.

Although the Kuroshio is known to alter how the internal tides in LS propagate and dissipate, how the internal tides interact with each other or with the subtidal circulation has not been well-documented (Kerry et al., 2013, 2014; Niwa & Hibiya, 2001). One important gap in knowledge exists: how the energy budget of the internal tides around LS relates to the interaction between the internal tide and the Kuroshio, and, in particular, how the internal tide radiates in response to the different Kuroshio paths (Alford et al., 2015; Y. Wang et al., 2018; Xu et al., 2014, 2016). A coordinated observation-modeling-theory study would advance our understanding of how the Kuroshio and internal tides interact with each other and the inherent controlling physics.

2. Methods

2.1. China Sea Multi-Scale Ocean Modeling System

The China Sea Multi-scale Ocean Modeling System (CMOMS, https://odmp.ust.hk/cmoms/) is an observationally and physically well-validated regional ocean model (Gan, Liu, & Liang, 2016; Gan, Liu, & Hui, 2016). The model has a horizontal resolution of about 0.1° and 30 vertical levels over the stretched terrain-following coordinates. With a novel open boundary condition (Liu & Gan, 2016) that accommodates tidal and subtidal forcing and considers regional circulation dynamics, the model well simulates the tidal signal and subtidal circulation in the SCS and adjacent ocean (Liu & Gan, 2017; Zu et al., 2008). We initialized the model with the WOA13 hydrographic field and spun it up for 50 years to a quasi-steady state with climatological atmospheric and lateral fluxes. Compared to existing models, CMOMS qualitatively and quantitatively resolves the nature of the Kuroshio and its variable intrusive pathways within LS (Figure 2).

In this study, we use the CMOMS to investigate the radiated internal tides modulated by the Kuroshio Current. The internal tide energy radiated away from the generation sites is mainly retained in low-mode (mode-1 and mode-2) internal tides that have relative longer wavelengths (Alford, 2003; Zhao et al., 2016). The mode-1 semidiurnal and diurnal internal tide wavelengths are respectively about 150 and 200 km in the study area, while the mode-2 semidiurnal and diurnal internal tide wavelengths are respectively about 70 and 100 km. With resolution ~0.1° (9–11 km), the lower-mode internal tides can be well resolved by the CMOMS (Figures 1 and 2).

2.2. Calculating the Group Velocity and Phase Speed

We calculated the eigenspeed, C, using the Taylor-Goldstein equation,

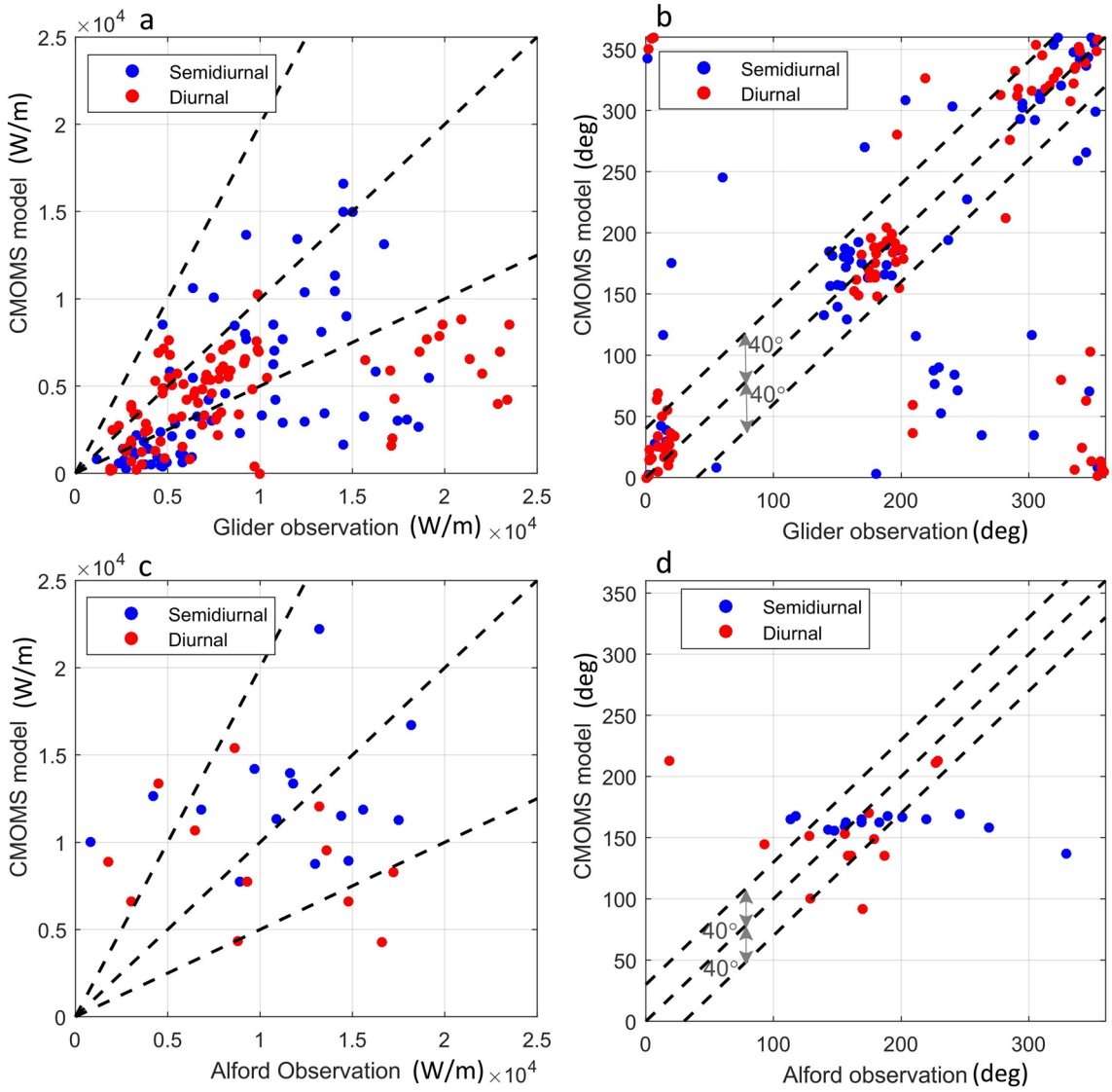

Figure 1. Comparison of glider-observed time-mean energy flux (Rainville et al., 2013) and modeled time-mean energy flux in (a) magnitudes of the energy flux from glider observations (*x* axis) and modeled values (*y* axis). The upper and lower dashed lines indicate the range of "a factor of two" and "one half", respectively; and (b) observed energy flux (*x* axis) and modeled directions (*y* axis). The upper and lower lines indicate the ±40° range, respectively. The red dots refer to diurnal and blue dots to semidiurnal internal tides. Comparison of observed (Alford et al., 2011) and modeled energy fluxes in (c) magnitudes of the energy flux from observations (*x* axis) and modeled values (*y* axis). The upper and lower dashed lines indicate the range of "a factor of two" and "one half", respectively; and (d) observed directions of the energy flux (*x* axis) and modeled directions (*y* axis). The upper and lower lines indicate the ±40° range, respectively. The red dots refer to diurnal and blue dots to semidiurnal internal tides.

$$\frac{d^2\hat{w}}{dz^2}+\left[\frac{N^2}{\left(U-C\right)^2}-\left|k\right|^2-\frac{d^2U\,/\,dz^2}{U-C}\right]\hat{w}=0 \tag{1}$$

where $\hat{w}$ is the eigenfunction of vertical velocity, and $U(z)$ is the background current. N is the buoyancy frequency that represents the stratification, and $\boldsymbol{k}=\left(k,l\right)$ is the horizontal wave number.

If we set $U(z)$ in Equation 1 equal to zero, N would determine C in the numerical solution of the equation. In that case, the effects of the background current would be absent, and we called this solution the "without-current-effect" C.

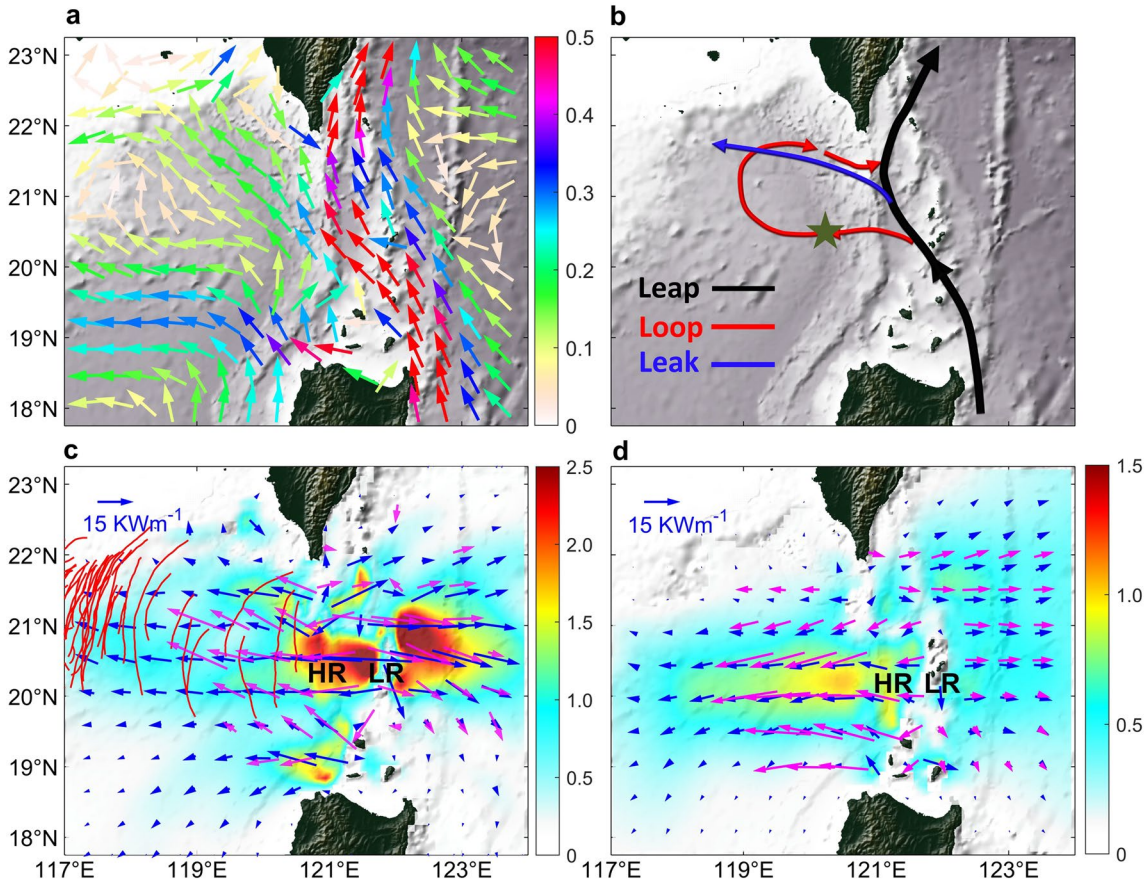

Figure 2. (a) Modeled long-term (2009–2010) mean Kuroshio patterns. The arrows indicate the direction of the current. The colors represent the magnitude of the current (Unit: m/s). (b) Sketched map of the three Kuroshio paths. The bold black curve represents the leaping path, the red dashed line is the looping path, and the blue dashed line is the leaking path. (c) Long-term mean simulated semidiurnal energy flux (blue arrows, unit: KW/m). The color contours represent the energy flux magnitude divided by 10^4 versus values observed by gliders (magenta arrows, data extracted from Figure 11 of Rainville et al. (2013), as the unique available in situ observed data set for energy flux field here). The red curves indicate the internal solitary waves observed in satellite images (extracted from Figure 7 of Zhao et al., 2014). (d) Same as (c) but for diurnal internal tides. HR depicts the Hengchun Ridge, and LR depicts the Lanyu Ridge.

If we consider the effects of the Earth's rotation, the group velocity without the effects of the background current becomes

$$\boldsymbol{c}_{g0}(x,y) = \frac{\sqrt{\omega^2 - f^2}}{\omega} c(x,y)\boldsymbol{k} \tag{2}$$

where $\boldsymbol{k}$ is the unit vector in the direction of the wave energy propagation, and $\boldsymbol{C}$ is still the eigenspeed (Alford & Zhao, 2007).

Then, if we now consider the background current, the "with-current-effect" group velocity would be (Kunze, 1985)

$$\boldsymbol{c}_g(x,y) = \boldsymbol{c}_{g0}(x,y) + \boldsymbol{U} \tag{3}$$

where $\boldsymbol{U}$ is the depth-averaged horizontal velocity within the upper water column with strong vertical shear of the Mode 1 internal tide.

The "with-current-effect" group velocity $\boldsymbol{c}_g(x,y)$ involves the refracting effects of the stratification and current, and we determine the "without-current-effect" group velocity, $\boldsymbol{c}_{g0}(x,y)$, only by the varying stratification $\boldsymbol{N}(x, y, z)$. In the following sections, the group speed represents the magnitude of the group velocity.

By setting the depth-dependent $U(z)$ to be zero or CMOMS output subtidal currents in equation (1) at each grid point, we get the "without-current-effect" and "with-current-effect" phase speeds (Alford et al., 2010; Li et al., 2016; Park & Farmer, 2013):

$$c_p(x,y) = \sqrt{\frac{\omega^2}{\omega^2 - \mathrm{f}^2}} C(x,y)\mathrm{k} \tag{4}$$

We use the phase speed of the first mode to calculate the wave path because the first mode accounts for most of the radiating internal tide energy.

This theoretical analysis based on the Taylor-Goldstein equation, with a correction for the Earth's rotation, clarifies the refraction mechanism that controls how the internal tide radiates within oceanic general circulation. There are plans to provide a more accurate estimate based on the full-mode equations (Duda et al., 2018; Huang et al., 2018).

2.3. Energy Ray-Tracing Model

We used the ray-tracing method, which is based on the Wentzel-Kramers-Brillouin (WKB) approximation, to investigate how internal waves interact with the background currents (Jones, 1969; Olbers, 1981). The WKB approximation assumes that the ratio of the internal wave scale to the scale of the background current is small. Dunphy (2014) found that the ray-tracing is invalid for reproducing internal tide propagation through an eddy if the ratio λ/L (wavelength/length scale of eddy) >1. However, many studies have shown that the ray-tracing method can be applied when the internal waves have wavelengths of the same order or even larger than the scale of the background currents. Kunze (1985) found that the ray-tracing method produced qualitatively consistent results with numerical solutions for near-inertial waves propagating through linear jets, when waves reflect due to a horizontal critical layer, and when the waves stall due to a vertical critical layer. Park and Watts (2006) and Rainville and Pinkel (2006) used the 2D ray-tracing method to study how mesoscale currents in the Japan Sea and Hawaii region modulate the semidiurnal internal tides. These researchers found that the ray-tracing results agreed qualitatively with observations. Chavanne et al. (2010) further used 3D ray-tracing to interpret the interaction of the semidiurnal internal tide with a surface-intensified cyclonic eddy.

For our study, we derived the energy ray solutions according to the ray equations (Duda et al., 2018),

$$\frac{dx}{ds} = Q\left[S(\alpha)\cos\alpha + \sin\alpha \left.\frac{\partial S}{\partial \theta}\right|_{\theta=\alpha}\right], \tag{5}$$

$$\frac{dy}{ds} = Q\left[S(\alpha)\sin\alpha - \cos\alpha \left.\frac{\partial S}{\partial \theta}\right|_{\theta=\alpha}\right], \tag{6}$$

$$\frac{dp_x}{ds} = QS(\alpha)\frac{\partial S}{\partial x}, \tag{7}$$

$$\frac{dp_y}{ds} = QS(\alpha)\frac{\partial S}{\partial y}, \tag{8}$$

$$\tan\beta = \frac{\left[S(\alpha)\sin\alpha - \cos\alpha \left.\frac{\partial S}{\partial \theta}\right|_{\theta=\alpha}\right]}{\left[S(\alpha)\cos\alpha + \sin\alpha \left.\frac{\partial S}{\partial \theta}\right|_{\theta=\alpha}\right]} = \frac{c_{gx}}{c_{gy}}, \tag{9}$$

where $S = \mathbf{k} / \omega$ is the slowness vector. α is the direction of the phase speed, and β is the direction of the internal tide energy. Q is the normalization factor. ds is the integration arc length increment. c_{gx} and c_{gy} are the

group speeds in zonal and meridional directions, respectively. With these five ray equations, we computed the theoretical energy ray trajectories of the internal tide.

2.4. Wavefront Tracing Model

The distance, Δd, that a wavefront propagates during a time interval, Δt, is

$$\Delta d = c_p \frac{\nabla \mathrm{s}}{|\nabla s|} \Delta t \tag{10}$$

where s is the normal vector of the wavefront, and thus, $\frac{\nabla s}{|\nabla s|}$ determines the propagation direction of the wavefront. We obtained the theoretical wave path (wavefront path) of the internal tide basing our computations on our calculated phase speeds (Alford et al., 2015; Li et al., 2016; Park & Farmer, 2013; Sherwin et al., 2002).

2.5. Model Validation

2.5.1. Observed Evidence for the Long-Term Mean

One of the most distinct outcomes of our study, compared with previous results, is that our simulated internal tide energy fluxes agree well in magnitude and direction with one-year mean glider observations (Rainville et al., 2013; magenta arrows in Figures 2c and 2d) and with satellite altimeter measurements (Zhao, 2014). We compare detailed observed and modeled time-mean energy fluxes in Figures 1a and 1b. We note that this is the first time that the model results have ever compared so well with this glider data (Figure 2). Compared to the magnitudes, the directions agree better with the data. The magnitudes of the simulated energy flux at some points are somewhat smaller than the glider values, which could have occurred for many reasons, such as errors in the glider observations and numerical approximation.

Furthermore, the northwestward semidiurnal beam is spatially coincident with the distribution of the internal solitary waves that we derived from multi-year Synthetic Aperture Radar images (Zhao et al., 2004; red curves in Figure 2c). The time-mean energy flux patterns and magnitude from our study also agree with previous tide-only forced simulations (Jan et al., 2008; Kerry et al., 2013; Niwa & Hibiya, 2004; X. Wang et al., 2016) and with observations (Klymak et al., 2011). The inferred magnitude of the internal tide's energy dissipation is about 10^{-2}–10^{-1} W/m^{-2}, which is consistent with observed (Klymak et al., 2011; St. Laurent, 2008; Tian et al., 2009) and simulated results (X. Wang et al., 2016). These close agreements gave us a high level of confidence to continue our study of how the internal tides interact with the Kuroshio in LS.

2.5.2. Observed Evidence for Specific Kuroshio Mode

Our model results compare favorably with the well-known and well-documented in situ baroclinic energy flux that Alford et al. (2011) observed. Specifically, our results for the leaping Kuroshio period show that our modeled and observed magnitudes of the energy fluxes are generally within a factor of two, and the energy flux directions generally agree within 40° (Figures 1c and 1d). Correctly resolving the Kuroshio pathways is crucial to capturing the internal tide's energetics and interpreting the underlying physics.

3. Results

3.1. Characteristics of the Kuroshio and Internal Tides in the LS

The Kuroshio is a major driver of the layered circulation in the SCS (Qu et al., 2004). As the Kuroshio moves through LS, its mainstream flows northward while approximately 20%–30% of its volume intrudes westward into the SCS (Figure 2a). The Kuroshio takes leaping, leaking, and looping paths through LS due to its strong, medium, and weak transports, respectively (Figure 2b; Nan et al., 2011; Zhang et al., 2017).

Barotropic tidal flows are amplified in LS due to the constriction of the strait. The barotropic flows interact with the local topography to generate prominent internal tides. Internal tides originating at LS radiate westward into the SCS and eastward into the northwestern Pacific Ocean (NPO). The internal tide energy flux

indicates where internal tides propagate to and where they dissipate. For our study, we derived the depth-integrated baroclinic energy flux of the internal tides following Kang and Fringer (2012).

Figures 2c and 2d show that the semidiurnal and diurnal internal tides have notably different patterns as they radiate toward the SCS. The energy flux associated with the semidiurnal internal tide bifurcates into a stronger beam originating at the middle of Lanyu Ridge and a weaker beam that radiates from the southern part of Lanyu Ridge (blue arrows in Figure 2c). The strong semidiurnal beam propagates northwestward toward the continental shelf of the SCS. In contrast, the diurnal beam mainly emanates from the middle and southern parts of Lanyu Ridge with a relatively uniform spatial pattern (blue arrows in Figure 2d) and radiates westward into the SCS from LS and then bends toward the equator in the deeper basin.

On the NPO side of LS, one semidiurnal and one diurnal beam are observed. Both beams are concentrated as they radiate with southward-bending patterns east of LS. The eastward (i.e., toward the NPO) diurnal beam is a little broader than the semidiurnal beam. The directions of the semidiurnal and diurnal beams propagating toward the NPO are almost perpendicular to the main flow of the Kuroshio, and the angles between the westward (i.e., toward the SCS) beams and the intrusive Kuroshio branch are much smaller than the angles of the eastward beams. Thus, the interaction between circulation and tides and the consequent tidal radiation patterns are distinctly different between the SCS and the NPO sides of LS. In the next section, we explain the underlying physics.

3.2. Internal Tide Response to the Kuroshio Paths

As we have mentioned, the Kuroshio intrudes into or bypasses LS along leaping, looping, and leaking paths (see Figure 2b). The leaping path corresponds to the strongest Kuroshio transport but is the weakest intrusion into the SCS and mostly occurs in summer. The looping path forms a strong anti-cyclonic pattern in winter in the northeastern SCS when the Kuroshio weakens. The leaking path is the most prevalent intrusion of the Kuroshio into the SCS.

With relatively high temperature and salinity, the varying Kuroshio alters the background current and the stratification, which affect the characteristics of the internal tide in the region. We compared the semidiurnal and diurnal internal tides corresponding to the Kuroshio's leaping (July 2010, which is the same period used by Alford et al., 2011) and looping (January 2010) paths (Figure 3). The internal tide's response to the leaking mode (not shown) is like the response to the leaping mode when the Kuroshio mainly flows northward in LS.

The eastward (i.e., toward the NPO) tidal beams under the leaping Kuroshio travel in similar directions and had similar widths as the beams under the looping Kuroshio; however, the beams radiating toward the SCS under these two modes have distinct features. For the leaping path, the semidiurnal and diurnal energy fluxes direct westward and were spatially constrictive (Figure 3). During the looping mode, the semidiurnal fluxes direct northwestward and southwestward through spatially spreading sub-beams. The diurnal beam also spreads under the refracting intrusive looping Kuroshio. Evidently, the tidal energy fluxes vary with the pathways of the Kuroshio in LS.

The magnitude of the tidal energy flux also has a close relationship with the stratification intensity. With the same topography and comparable barotropic tides (not shown), the changes in the internal tide magnitudes mainly result from stratification variability associated with a variable Kuroshio. The stratification in July 2010, when the leaping path dominated in LS, is much stronger than in January when the looping path dominated (Nan et al., 2011, Figures 3a and 3b). Consequently, the barotropic to baroclinic energy conversion rate and energy flux for the leaping path are much stronger than for the looping path, whereas the changing stratification has limited influence on the radiating pattern of internal tides.

In addition, we estimated the latitudinal geography of the radiating tidal energy modulated by the different Kuroshio paths. The latitudinal energy flux distributions within the tidal beams radiating toward the NPO remain nearly unchanged with the Kuroshio paths, the eastward energy is only slightly refracted northward under the leaping Kuroshio path (Figures 4c and 4d). However, the energy radiating toward the SCS remarkably varies latitudinally under the different Kuroshio paths (Figures 4c and 4d). The semidiurnal energy radiates relatively uniformly latitudinally toward the SCS for the leaping mode but is significantly

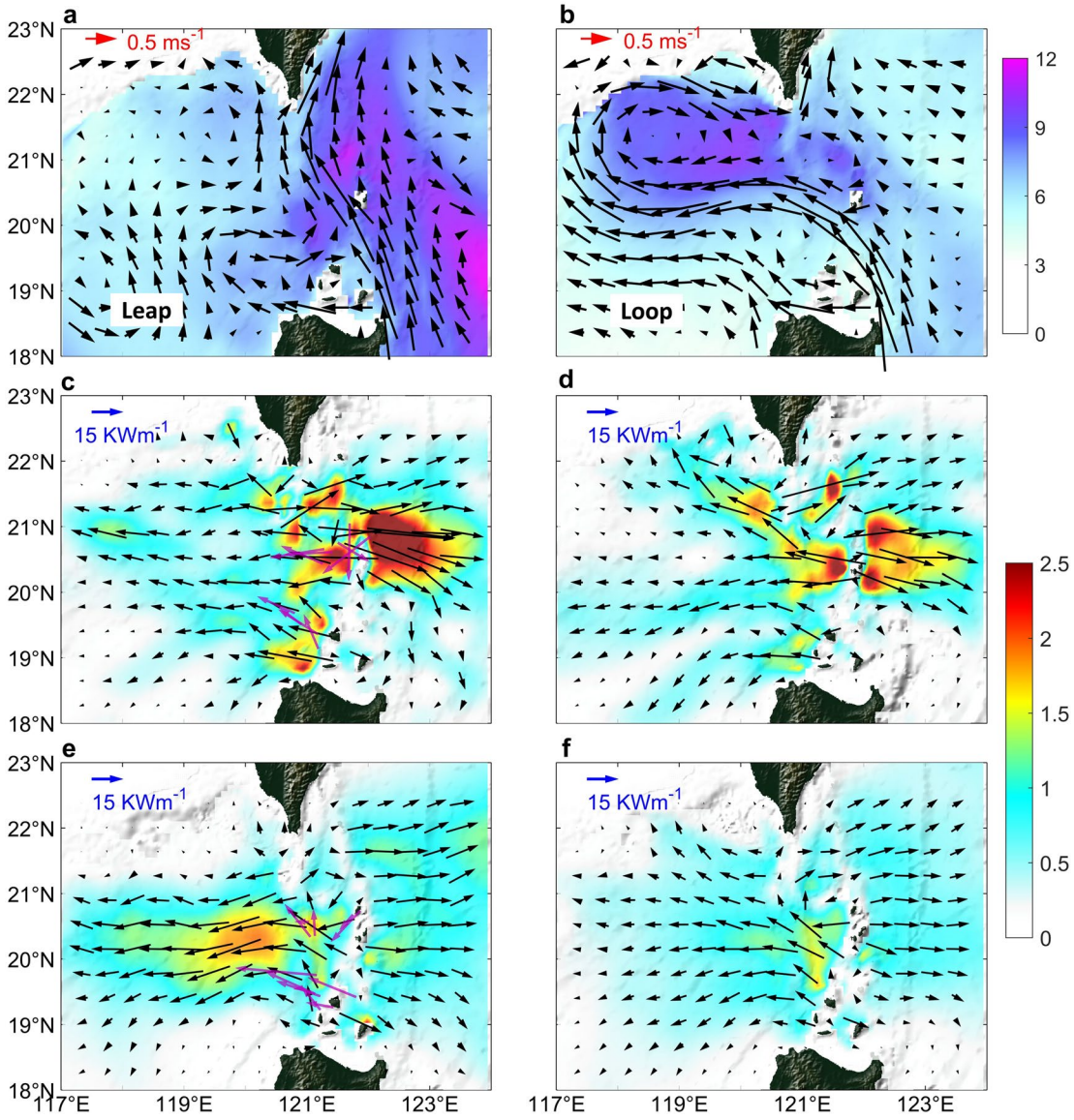

Figure 3. (a) Leaping path of the Kuroshio during July 2010. The color contours are the values of N^2 (multiplied by 10^5) representing the stratification at 200 m depth. The black arrows represent the currents (in m/s). (b) Same as (a) but for the looping path of the Kuroshio during January 2010. (c) Semidiurnal internal tide radiating pattern under the leaping Kuroshio path. The black arrows represent the simulated energy flux (in KW/m; colors represent the energy flux magnitude divided by 10^4), and the purple arrows indicate the observed values from Alford et al. (2011). (d) Semidiurnal internal tide radiating under the looping Kuroshio path. (e and f) As in (c and d) but for diurnal internal tides.

redistributed with more energy in the north for the looping Kuroshio. In contrast, a substantial percentage of the diurnal energy radiating toward the SCS for the leaping mode stays in the middle, while more diurnal energy flux broadly radiates along LS under the looping Kuroshio.

The different intruding paths of the Kuroshio significantly alter how the internal tide generates and alters the tidal energy paths as it radiates toward the SCS (Figures 4c and 4d). Consequently, the dissipation field in the Kuroshio is spatially complex and inhomogeneous, which crucially impacts the circulation's variability (Figure 4). On the other hand, it has recently been suggested that the local dissipation efficiency, q, varies spatially (Vic et al., 2019). The local dissipation efficiency is defined as the fraction of internal tide energy that dissipates near the source regions. The local dissipation efficiency is a cornerstone of tidal mixing parameterizations and is usually constant (i.e., 1/3) in ocean climate models.

The energy balance equation for the internal tide can be described as

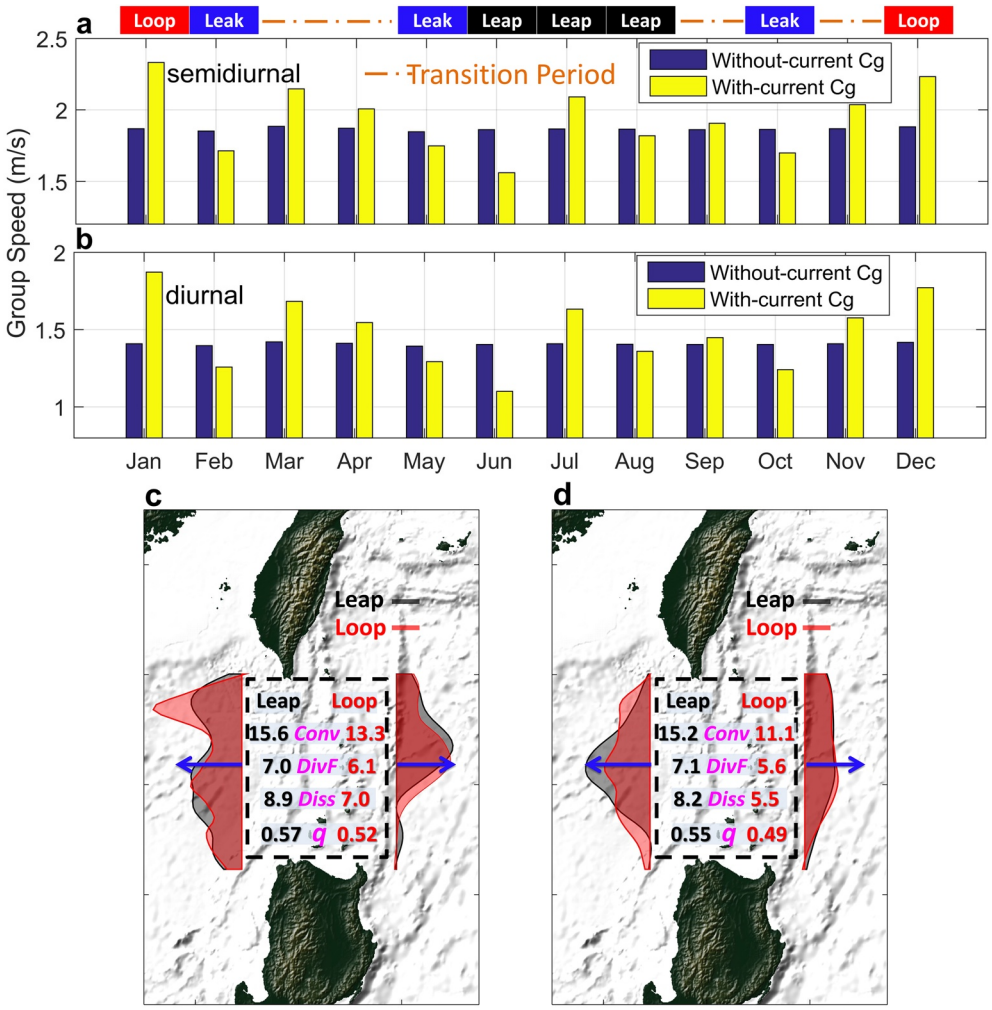

Figure 4. (a) Time series of semidiurnal group speed (magnitude of the group velocity) for the location marked by the green star in Figure 2b. The yellow bars represent the group speed under the influence of the subtidal current. The blue bars are for the group speed without the subtidal current. (b) Same as (a) but for diurnal internal tides. (c) The energetic budget and latitudinal distribution of the percentage of semidiurnal energy flux under the looping (red) and leaping (gray) Kuroshio paths. "Conv" indicates the barotropic to baroclinic conversion rate. "DivF" is the divergence of energy flux. "Diss" is the dissipating rate, and "q" is the local dissipation rate. The unit for the Conv, DivF, and Diss is GW. (d) Same as (c) but for diurnal internal tides.

$$\nabla_H \cdot \| \bar{F} \| = \| \bar{C} \| - \| \bar{D} + \bar{\varepsilon} \| \tag{11}$$

where the $\| \cdot \|$ represents time-average operator. The first term represents the divergence of the internal tide energy flux. The second term represents the converted energy from barotropic tide to internal tide, and the third term is the dissipation portion. Then, the local dissipation efficiency, q, is defined as

$$q = \frac{\int_s ds\left(\| \bar{D} + \bar{\varepsilon} \|\right)}{\int_s ds\left(\| \bar{C} \|\right)} \tag{12}$$

for which we found that q varies temporally relative to the varying background circulation. Here $\int_s$ indicates the area-integration at the Luzon Strait. Specially, q (for diurnal and semidiurnal tides) is larger with the leaping path than with the looping path of the Kuroshio. The intensified stratification of the leaping Kuroshio results in higher mode internal tides. The leaping Kuroshio, accompanied by larger current shear, also contributes to more local dissipation (higher q) of the internal tides near the source site.

3.3. Dynamics and Mechanisms

3.3.1. Variation of the Group Velocity

We calculated the group velocities with and without the effects of the background Kuroshio current. With these two separate cases, we assessed how much the current and stratification contributed to the variability of the group velocity relative to each other. We calculated the group velocity at a key location (green star in Figure 2b) on the main axis of the looping Kuroshio branch, which is where the semidiurnal beam radiating toward the SCS starts to split. At this location, the different Kuroshio paths influence the varying directions of the radiating beam.

It is evident that the group speed (magnitude of the group velocity) changes more significantly with the current present than without the current (Figures 4a and 4b). Moreover, the group speeds of the semidiurnal and diurnal internal tides vary similarly under the different Kuroshio paths. Specifically, for the looping path, the group speed (>2 m/s) is larger than for the leaping and leaking paths. These findings reinforce the notion that the background current is critical in modulating how the internal tide radiates at the periphery of LS.

3.3.2. Refraction Under the Looping and Leaping Kuroshio

The varying group velocity leads to distinct features in the radiating internal tides under the different Kuroshio paths. The horizontally inhomogeneous current could lead to an anisotropic group velocity and wavenumber of internal tides. The anisotropic group velocity indicates the refraction of internal tide energy. Specifically, the difference in the group velocities at different locations demonstrates the change in the wave energy's radiating direction.

To clarify the main physical process that accounts for the refraction, we analyzed the spatial distribution of the group speed anomaly (deviation from the long-term mean). We present only the semidiurnal group speed anomalies of our analysis in Figures 5a–5d. For the leaping and looping paths, the anomalies for when the Kuroshio was present are much larger than without the influence of the Kuroshio. Clearly, the group speed anomalies and associated variations in the propagation direction of the internal tides are influenced more by the background Kuroshio Current than by the stratification.

The group speed anomalies when we considered the background current have complex distributions corresponding to the leaping and looping Kuroshio paths. On the SCS side, the group speed anomalies for the looping path are much larger than for the leaping path, which indicates that the looping Kuroshio Current refracts the internal tide more than the leaping current does (Figures 5a and 5b). However, on the NPO side, the leaping and looping Kuroshio have a weak effect on group speed anomalies in the eastward tidal beams. The intrusive component of the Kuroshio aligning with the tidal energy flux direction effectively alters the group speed variation on the SCS side. In contrast, the Kuroshio flows almost perpendicularly toward the eastward internal tide beam on the NPO side.

3.3.3. Theoretical Wave Tracing

First, we calculated the theoretical energy radiating rays of internal tides using the ray-tracing method. We only show the ray-tracing results for the semidiurnal internal tides that propagate toward the SCS (black lines in Figures 5a–5d). The energy rays without the current exhibit similar spatial paths for the leaping and looping Kuroshio modes. The slight difference is due to the varying stratification distribution. With the influence of the background current, however, the energy ray trajectories have distinct spreading paths. In particular, the looping intrusive Kuroshio branch significantly shifts the energy rays northward and southward, which is consistent with the simulated energy flux pattern. The ray-tracing results are qualitatively consistent to the modeled patterns, which confirms the suitability of using the ray-tracing method in our study.

Next, we obtained the propagation pattern of the internal tide wavefront by using the distribution of the calculated phase speed. We integrated theoretical wave pattern for the cases with and without the background current for the tidal beams radiating toward the SCS. The propagation pattern of the internal tide wavefront agrees quite well with the direction of the energy ray. The leaping and looping Kuroshio lead to more spread

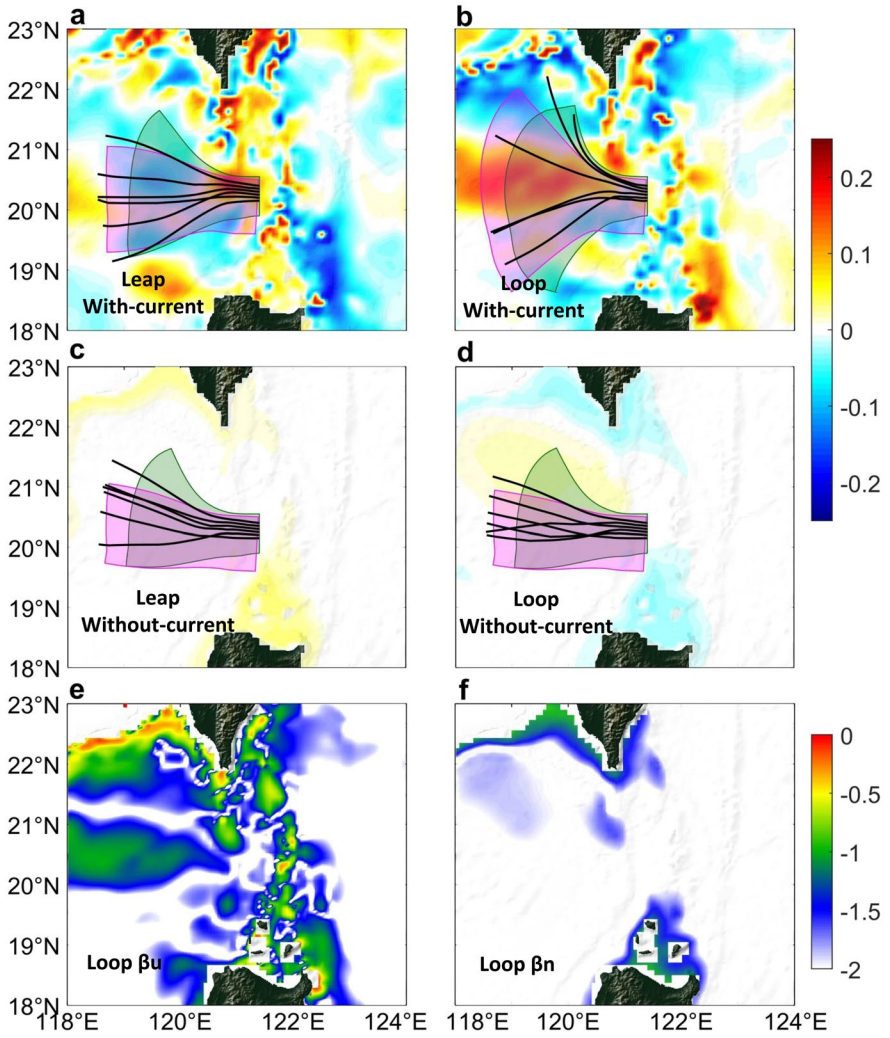

Figure 5. (a) The colors indicate the calculated semidiurnal group speed (magnitude of the group velocity) anomalies (in m/s) for the leaping Kuroshio path. The black lines indicate the energy radiating path of semidiurnal internal tide derived from the ray-tracing model based on group speed distribution. The plane-wave radiation paths derived from the wave-tracing model based on phase speed are green and magenta representing semidiurnal and diurnal internal tides, respectively. (b) Same as (a) but for the looping Kuroshio path. (c and d) Same as (a and b) but for the case without the current effect. (e and f) β_U and β_N calculated according to Equations 13 and 14 for the looping Kuroshio path. Note that the color bar is in log10 scale.

in the patterns of the internal tide crests, while the waveforms in the without-current-effect case converge more. Like the raypath, the looping Kuroshio forms a stronger spreading wave front.

3.3.4. Criterion for Relative Contributions

Background currents, stratification intensity, and the mean internal tide propagation patterns vary from location to location. We calculated the relative contributions of the current and stratification to the radiating internal tide as follows:

$$\beta_U = \frac{\left|c_{gU} - c_{g0}\right|}{c_{g0}} \tag{13}$$

$$\beta_N = \frac{\left|c_{gN} - c_{g0}\right|}{c_{g0}} \tag{14}$$

c_{gU} and c_{gN} are the magnitudes of group velocity with and without considering the background current, respectively. c_{g0} represents the long-term mean magnitude of group velocity. By calculating and comparing the parameters, β_U and β_N, we determined if it is the current or the stratification that influences the temporal variation of the tidal radiation path more.

On the SCS side, the overall β_U is approximately 10^{-1}. In contrast, β_N on the SCS side is generally smaller than 10^{-2}, except over the continental shelf where the contribution of stratification to internal tide radiation is about several percent. In general, the background intrusive current contributes tens of percent to the phase speed variation. On the NPO side, β_U and β_N are mostly below 10^{-2}, suggesting that neither the background current nor the stratification significantly refract the internal tide radiation.

4. Discussion and Conclusion

In this study, we used a well-validated numerical model to provide new insights into the characteristics, variation, and underlying dynamics of the internal tide's energy field near LS. With the model results, we investigated the responses of the internal tides to the background Kuroshio Current. Our goal was to fill the knowledge gaps of the Kuroshio Current's influence on the radiation and energy pathways, and the underlying physics of the internal tides.

We saw that the Kuroshio significantly influences the radiation pattern and magnitude of the internal tides that vary spatiotemporally with the leaping, looping, and leaking paths of the Kuroshio around LS. The Kuroshio paths largely modulate the energy budget and latitudinal distribution of the internal tide energy flux. We found that the background current plays a leading role in modulating how the internal tide radiates, and that the variable stratification only slightly influences the radiation pattern around LS. We proposed a criterion of global significance for evaluating the relative importance of the current and stratification with regards to internal tide refraction.

The Northwestern Pacific Ocean Circulation and Climate Experiment (Hu et al., 2015) recently reviewed many existing models and found they poorly resolved circulation in marginal seas where there are complex terrain and intrinsic and extrinsic forcings. The accuracy of the well-validated CMOMS is partially attributed to its well-represented tidal and subtidal dynamics and multiscale interactions in regional ocean circulation.

Our study provided a new dynamic insight on how subtidal currents modulate the spatiotemporal variability of internal tides, which is important for diagnosing the balanced motions and unbalanced internal waves in the real ocean, for identifying energy transfer and redistribution in long-range radiated internal tides, and for improving subscale parameterization in climate-scale ocean circulation models.

CMOMS's ability to reproduce the large-scale circulation field and internal tide's energy field has been well-validated. Model physics, physical-numerical accommodated simulation schemes, resolution, and other sensible implementations (e.g., tidal-subtidal open boundary condition adopted in Liu & Gan, 2017) all matter in determining how well the model performs and deserve further investigation in the future studies.

We calculated the eigenspeed and resultant group velocity and phase speed by solving the Taylor-Goldstein mode equation in this current study. This study mainly focused on the key dynamics and mechanisms that govern the interactions between internal tides and the Kuroshio. In the future, we plan to calculate the full-mode equations involving the simulated and measured shear current to clarify and quantify the refraction mechanism that controls how the internal tide radiates within general oceanic circulation.

Data Availability Statement

The data used in this study are available in the CMOMS web site at https://odmp.ust.hk/cmoms/?page_id=453.

Acknowledgments
Xu Zhenhua was supported by the Strategic Pioneering Research Program of CAS, the National Natural Science Foundation of China, the National Key Research and Development Program of China (XDB42000000, 2017YFA0604102, 92058202, XDA22050202, 2016YFC1401404, 91858103, 42006031), CAS Key Research Program of Frontier Sciences and Key Deployment Project of Centre for Ocean Mega-Research of Science (QYZDB-SSW-DQC024, COMS2020Q07). Gan Jianping was supported by the Hong Kong Research Grants Council (GRF16204915, 16212720).

References

Alford, M. H. (2003). Redistribution of energy available for ocean mixing by long-range propagation of internal waves. *Nature*, *423*(6936), 159–162. https://doi.org/10.1038/nature01628

Alford, M. H., Lien, R. C., Simmons, H., Klymak, J., Ramp, S., Yang, Y. J., et al. (2010). Speed and evolution of nonlinear internal waves transiting the South China Sea. *Journal of Physical Oceanography*, *40*(6), 1338–1355. https://doi.org/10.1175/2010jpo4388.1

Alford, M. H., MacKinnon, J. A., Simmons, H., Pickering, A., Klymak, J. M., et al. (2011). Energy flux and dissipation in Luzon Strait: Two tales of two ridges. *Journal of Physical Oceanography*, *41*, 2211–2222. https://doi.org/10.1175/jpo-d-11-073.1

Alford, M. H., Peacock, T., MacKinnon, J. A., Nash, J. D., Buijsman, M. C., Centurioni, L. R., et al. (2015). The formation and fate of internal waves in the South China Sea. *Nature*, *521*, 65–69. https://doi.org/10.1038/nature14399

Alford, M. H., & Zhao, Z. (2007). Global patterns of low-mode internal-wave propagation. Part II: group velocity. *Journal of Physical Oceanography*, *37*(7), 1849–1858. https://doi.org/10.1175/jpo3086.1

Buijsman, M. C., Kanarska, Y., & McWilliams, J. C. (2010). On the generation and evolution of nonlinear internal waves in the South China Sea. *Journal of Geophysical Research*, *115*, C02012. https://doi.org/10.1029/2009jc005275

Buijsman, M. C., McWilliams, J. C., & Jackson, C. R. (2010). East-west asymmetry in nonlinear internal waves from Luzon Strait. *Journal of Geophysical Research*, *115*, C10057. https://doi.org/10.1029/2009JC006004

Chang, H., Xu, Z., Yin, B., Hou, Y., Liu, Y., Li, D., et al. (2019). Generation and propagation of M2 internal tides modulated by the Kuroshio northeast of Taiwan. *Journal of Geophysical Research: Oceans*, *124*, 2728–2749. https://doi.org/10.1029/2018JC014228

Chavanne, C., Flament, P., Luther, D., & Gurgel, K. W. (2010). The surface expression of semidiurnal internal tides near a strong source at Hawaii. Part II: Interactions with mesoscale currents. *Journal of Physical Oceanography*, *40*(6), 1180–1200. https://doi.org/10.1175/2010jpo4223.1

Duda, T. F., Lin, Y., Buijsman, M., & Newhall, A. E. (2018). Internal tidal modal ray refraction and energy ducting in baroclinic Gulf Stream currents. *Journal of Physical Oceanography*, *48*, 1969–1993. https://doi.org/10.1175/jpo-d-18-0031.1

Dunphy, M. (2014). *Focusing and vertical mode scattering of the first mode internal tide via mesoscale eddy interactions*. UWSpace. Retrieved from https://uwspace.uwaterloo.ca/handle/10012/8865

Dunphy, M., & Lamb, K. G. (2014). Focusing and vertical mode scattering of the first mode internal tide by mesoscale eddy interaction. *Journal of Geophysical Research: Oceans*, *119*, 523–536. https://doi.org/10.1002/2013JC009293

Gan, J., Liu, Z., & Hui, C. R. (2016). A three-layer alternating spinning circulation in the South China Sea. *Journal of Physical Oceanography*, *46*, 2309–2315. https://doi.org/10.1175/jpo-d-16-0044.1

Gan, J., Liu, Z., & Liang, L. (2016). Numerical modeling of intrinsically and extrinsically forced seasonal circulation in the China seas: A kinematic study. *Journal of Geophysical Research: Oceans*, *121*, 4697–4715. https://doi.org/10.1002/2016jc011800

Garrett, C., & Kunze, E. (2007). Internal tide generation in the deep ocean. *Annual Review of Fluid Mechanics*, *39*, 57–87. https://doi.org/10.1146/annurev.fluid.39.050905.110227

Hu, D., Wu, L., Cai, W., Gupta, A. S., Ganachaud, A., Qiu, B., et al. (2015). Pacific western boundary currents and their roles in climate. *Nature*, *522*, 299–308. https://doi.org/10.1038/nature14504

Huang, X., Wang, Z., Zhang, Z., Yang, Y., Zhou, C., Yang, C., et al. (2018). Role of mesoscale eddies in modulating the semidiurnal internal tide: Observation results in the northern South China Sea. *Journal of Physical Oceanography*, *48*, 1749–1770. https://doi.org/10.1175/jpo-d-17-0209.1

Jan, S., Chern, C. S., Wang, J., & Chiou, M. D. (2012). Generation and propagation of baroclinic tides modified by the Kuroshio in the Luzon Strait. *Journal of Geophysical Research*, *117*, C00027. https://doi.org/10.1029/2011JC007229

Jan, S., Lien, R. C., & Ting, C. H. (2008). Numerical study of baroclinic tides in Luzon Strait. *Journal of Oceanography*, *64*(5), 789–802. https://doi.org/10.1007/s10872-008-0066-5

Jones, W. L. (1969). Ray tracing for internal gravity waves. *Journal of Geophysical Research*, *74*(8), 2028–2033. https://doi.org/10.1029/jb074i008p02028

Kang, D., & Fringer, O. (2012). Energetics of barotropic and baroclinic tides in the Monterey Bay area. *Journal of Physical Oceanography*, *42*, 272–290. https://doi.org/10.1175/jpo-d-11-039.1

Kelly, S. M., Lermusiaux, P. F., Duda, T. F., & Haley, P. J., Jr. (2016). A coupled-mode shallow-water model for tidal analysis: Internal tide reflection and refraction by the Gulf Stream. *Journal of Physical Oceanography*, *46*, 3661–3679. https://doi.org/10.1175/jpo-d-16-0018.1

Kerry, C. G., Powell, B. S., & Carter, G. S. (2013). Effects of remote generation sites on model estimates of M2 internal tides in the Philippine Sea. *Journal of Physical Oceanography*, *43*(1), 187–204. https://doi.org/10.1175/jpo-d-12-081.1

Kerry, C. G., Powell, B. S., & Carter, G. S. (2014). The impact of subtidal circulation on internal tide generation and propagation in the Philippine Sea. *Journal of Physical Oceanography*, *44*, 1386–1405. https://doi.org/10.1175/jpo-d-13-0142.1

Klymak, J. M., Alford, M. H., Pinkel, R., Lien, R. C., Yang, Y. J., & Tang, T. Y. (2011). The breaking and scattering of the internal tide on a continental slope. *Journal of Physical Oceanography*, *41*(5), 926–945. https://doi.org/10.1175/2010jpo4500.1

Koch-Larrouy, A., Lengaigne, M., Terray, P., Madec, G., & Masson, S. (2010). Tidal mixing in the Indonesian seas and its effect on the tropical climate system. *Climate Dynamics*, *34*(6), 891–904. https://doi.org/10.1007/s00382-009-0642-4

Kunze, E. (1985). Near-inertial wave propagation in geostrophic shear. *Journal of Physical Oceanography*, *15*(5), 544–565. https://doi.org/10.1175/1520-0485(1985)015<0544:niwpig>2.0.co;2

Li, Q., Wang, B., Chen, X., Chen, X., & Park, J.-H. (2016). Variability of nonlinear internal waves in the South China Sea affected by the Kuroshio and mesoscale eddies. *Journal of Geophysical Research: Oceans*, *121*(4). https://doi.org/10.1002/2015JC011134

Liu, Z., & Gan, J. (2016). Open boundary conditions for tidally and subtidally forced circulation in a limited-area coastal model using the Regional Ocean Modeling System (ROMS). *Journal of Geophysical Research: Oceans*, *121*, 6184–6203. https://doi.org/10.1002/2016JC011975

Liu, Z., & Gan, J. (2017). Three-dimensional pathways of water masses in the South China Sea: A modeling study. *Journal of Geophysical Research: Oceans*, *122*, 6039–6054. https://doi.org/10.1002/2016jc012511

McWilliams, J. C. (2016). Submesoscale currents in the ocean. *Proceedings of the Royal Society A*, *472*, 20160117. https://doi.org/10.1098/rspa.2016.0117

Nan, F., Xue, H., Chai, F., Shi, L., Shi, M., & Guo, P. (2011). Identification of different types of Kuroshio intrusion into the South China Sea. *Ocean Dynamics*, *61*, 1291–1304. https://doi.org/10.1007/s10236-011-0426-3

Niwa, Y., & Hibiya, T. (2001). Numerical study of the spatial distribution of the M2 internal tide in the Pacific Ocean. *Journal of Geophysical Research*, *106*, 22441–22449. https://doi.org/10.1029/2000jc000770

Niwa, Y., & Hibiya, T. (2004). Three-dimensional numerical simulation of M2 internal tides in the East China Sea. *Journal of Geophysical Research*, *109*(C4). https://doi.org/10.1029/2003JC001923

Olbers, D. J. (1981). The propagation of internal waves in a geostrophic current. *Journal of Physical Oceanography*, *11*(9), 1224–1233. https://doi.org/10.1175/1520-0485(1981)011<1224:tpoiwi>2.0.co;2

Park, J. H., & Farmer, D. (2013). Effects of Kuroshio intrusions on nonlinear internal waves in the South China Sea during winter. *Journal of Geophysical Research: Oceans*, *118*, 7081–7094. https://doi.org/10.1002/2013jc008983

Park, J. H., & Watts, D. R. (2006). Internal tides in the southwestern Japan/East Sea. *Journal of Physical Oceanography*, *36*(1), 22–34. https://doi.org/10.1175/jpo2846.1

Pickering, A., Alford, M., Nash, J., Rainville, L., Buijsman, M., Ko, D. S., & Lim, B. (2015). Structure and variability of internal tides in Luzon Strait. *Journal of Physical Oceanography*, *45*, 1574–1594. https://doi.org/10.1175/jpo-d-14-0250.1

Polzin, K. L., Toole, J. M., Ledwell, J. R., & Schmitt, R. W. (1997). Spatial variability of turbulent mixing in the abyssal ocean. *Science*, *276*, 93–96. https://doi.org/10.1126/science.276.5309.93

Qiu, B., Nakano, T., Chen, S., & Klein, P. (2017). Submesoscale transition from geostrophic flows to internal waves in the northwestern Pacific upper ocean. *Nature Communication*, *8*, 14055. https://doi.org/10.1038/ncomms14055

Qu, T., Kim, Y. Y., Yaremchuk, M., Tozuka, T., Ishida, A., & Yamagata, T. (2004). Can Luzon Strait transport play a role in conveying the impact of ENSO to the South China Sea? *Journal of Climate*, *17*, 3644–3657. https://doi.org/10.1175/1520-0442(2004)017<3644:clstpa>2.0.co;2

Rainville, L., Lee, C. M., Rudnick, D. L., & Yang, K. C. (2013). Propagation of internal tides generated near Luzon Strait: Observations from autonomous gliders. *Journal of Geophysical Research: Oceans*, *118*, 4125–4138. https://doi.org/10.1002/jgrc.20293

Rainville, L., & Pinkel, R. (2006). Propagation of low-mode internal waves through the ocean. *Journal of Physical Oceanography*, *36*(6), 1220–1236. https://doi.org/10.1175/JPO2889.1

Sherwin, T. J., Vlasenko, V. I., Stashchuk, N., Jeans, D. R. G., & Jones, B. (2002). Along-slope generation as an explanation for some unusually large internal tides. *Deep Sea Research Part I: Oceanographic Research Papers*, *49*(10), 1787–1799. https://doi.org/10.1016/s0967-0637(02)00096-1

Sprintall, J., Gordon, A. L., Koch-Larrouy, A., Lee, T., Potemra, J. T., Pujiana, K., & Wijffels, S. E. (2014). The Indonesian Seas and their impact on the coupled ocean climate system. *Nature Geoscience*, *7*, 487–492. https://doi.org/10.1038/NGEO2188

St Laurent, L. (2008). Turbulent dissipation on the margins of the South China Sea. *Geophysical Research Letters*, *35*(23). https://doi.org/10.1029/2008GL035520

Susanto, R. D., Gordon, A. L., & Sprintall, J. (2007). Observations and proxies of the surface layer throughflow in Lombok Strait. *Journal of Geophysical Research*, *112*, C03S92. https://doi.org/10.1029/2006JC003790

Tian, J., Yang, Q., & Zhao, W. (2009). Enhanced diapycnal mixing in the South China Sea. *Journal of Physical Oceanography*, *39*(12), 3191–3203. https://doi.org/10.1175/2009jpo3899.1

Varlamov, S. M., Guo, X., Miyama, T., Ichikawa, K., Waseda, T., & Miyazawa, Y. (2015). M2 baroclinic tide variability modulated by the ocean circulation south of Japan. *Journal of Geophysical Research: Oceans*, *120*. https://doi.org/10.1002/2015JC010739

Vic, C., Naveira Garabato, A. C., Mattias Green, J. A., Waterhouse, A. F., Zhao, Z., Melet, A., et al. (2019). Deep-ocean mixing driven by small-scale internal tides. *Nature Communications*, *10*, 2099. https://doi.org/10.1038/s41467-019-10149-5

Vlasenko, V., Stashchuk, N., & Hutter, K. (2005). *Baroclinic tides: Theoretical modeling and observational evidence*. Cambridge University Press. https://doi.org/10.1017/cbo9780511535932

Wang, X., Peng, S., Liu, Z., Huang, R. X., Qian, Y. K., & Li, Y. (2016). Tidal mixing in the South China Sea: An estimate based on the internal tide energetics. *Journal of Physical Oceanography*, *46*(1), 107–124. https://doi.org/10.1175/jpo-d-15-0082.1

Wang, Y., Xu, Z., Yin, B., Hou, Y., & Chang, H. (2018). Long-range radiation and interference pattern of multisource M2 internal tides in the Philippine Sea. *Journal of Geophysical Research: Oceans*, *123*, 5091–5112. https://doi.org/10.1029/2018jc013910

Whalen, C. B., MacKinnon, J. A., & Talley, L. D. (2018). Large-scale impacts of the mesoscale environment on mixing from wind-driven internal waves. *Nature Geoscience*, *11*, 842–847. https://doi.org/10.1038/s41561-018-0213-6

Xu, Z., Liu, K., Yin, B., Zhao, Z., Wang, Y., & Li, Q. (2016). Long-range propagation and associated variability of internal tides in the South China Sea. *Journal of Geophysical Research: Oceans*, *121*, 8268–8286. https://doi.org/10.1002/2016jc012105

Xu, Z., Yin, B., Hou, Y., & Liu, A. K. (2014). Seasonal variability and north–south asymmetry of internal tides in the deep basin west of the Luzon Strait. *Journal of Marine Systems*, *134*, 101–112. https://doi.org/10.1016/j.jmarsys.2014.03.002

Xu, Z., Yin, B. S., Hou, Y. J., & Xu, Y. S. (2013). Variability of internal tides and near-inertial waves on the continental slope of the northwestern South China Sea. *Journal of Geophysical Research: Oceans*, *118*, 197–211. https://doi.org/10.1029/2012JC008212

Zaron, E. D., & Egbert, G. D. (2014). Time-variable refraction of the internal tide at the Hawaiian Ridge. *Journal of Physical Oceanography*, *44*, 538–557. https://doi.org/10.1175/jpo-d-12-0238.1

Zhang, Z., Zhao, W., Qiu, B., & Tian, J. (2017). Anticyclonic eddy sheddings from Kuroshio loop and the accompanying cyclonic eddy in the northeastern South China Sea. *Journal of Physical Oceanography*, *47*(6), 1243–1259. https://doi.org/10.1175/jpo-d-16-0185.1

Zhao, Z. (2014). Internal tide radiation from the Luzon Strait. *Journal of Geophysical Research: Oceans*, *119*, 5434–5448. https://doi.org/10.1002/2014jc010014

Zhao, Z., Alford, M. H., Girton, J. B., Rainville, L., & Simmons, H. L. (2016). Global observations of open-ocean mode-1 M2 internal tides. *Journal of Physical Oceanography*, *46*, 1657–1684. https://doi.org/10.1175/jpo-d-15-0105.1

Zhao, Z., Klemas, V., Zheng, Q., & Yan, X.-H. (2004). Remote sensing evidence for baroclinic tide origin of internal solitary waves in the northeastern South China Sea. *Geophysical Research Letters*, *31*, L06302. https://doi.org/10.1029/2003GL019077

Zu, T., Gan, J., & Erofeeva, S. Y. (2008). Numerical study of the tide and tidal dynamics in the South China Sea. *Deep Sea Research Part I: Oceanographic Research Papers*, *55*, 137–154. https://doi.org/10.1016/j.dsr.2007.10.007